CHEMISTRY
A EUROPEAN JOURNAL

DOI: 10.1002/chem.201000560

Asymmetric Phase-Transfer-Catalyzed Intramolecular N-Alkylation of Indoles and Pyrroles: A Combined Experimental and Theoretical Investigation

Marco Bandini,*[a] Andrea Bottoni,[a] Astrid Eichholzer,[a] Gian Pietro Miscione,*[a] and Marco Stenta[b]

Abstract: Asymmetric phase-transfer catalysis (PTC) has risen to prominence over the last decade as a straightforward synthetic methodology for the preparation of pharmacologically active compounds in enantiomerically pure form. However, the complex interplay of weak nonbonded interactions (between catalyst and substrate) that could account for the stereoselection in these processes is still unclear, with tentative pictorial mechanistic representations usually proposed. Here we present a full account dealing with the enantioselective phase-transfer-catalyzed intramolecular aza-Michael reaction (IMAMR) of indolyl esters, as a valuable synthetic tool to obtain added-value compounds, such as dihydro-pyrazinoindolinones. A combined computational and experimental investigation has been carried out to elucidate the key mechanistic aspects of this process.

Keywords: asymmetric catalysis · computational chemistry · indoles · Michael addition · phase-transfer catalysis

Introduction

The indole nucleus represents a key molecular motif with widespread occurrence in nature and featuring peculiar pharmacological and agrochemical activities.[1] Accordingly, it is not surprising that a great deal of attention has been devoted to the use of innovative organic synthetic methodologies to prepare tailored synthetic indolyl-containing compounds.[2] Within these synthetic approaches, the development of enantioselective Friedel–Crafts alkylations (FCAs) has triggered increasing interest over the last few years, thanks to the growing availability of efficient chiral metal-based and metal-free catalysts.[3] Additions to carbonyl compounds, Michael additions to electron-deficient olefins, hydroarylations of unactivated C–C multiple bonds, and S_N2/S_N1 processes involving epoxides/π-activated alcohols deserve particular mention among the most reliable catalytic stereoselective FC-type processes.[4]

Indole is commonly referred to as an electron-rich (*generous*) heteroaromatic system, showing enhanced reactivity (compared to benzene) in electrophilic aromatic substitutions. It has been involved in nearly 70% of the reported examples addressing catalytic and stereoselective FCA processes with the quasi-exclusive functionalization of the most nucleophilic C3 position. On the other hand, direct C2-selective catalytic enantioselective alkylations of indoles is still an open synthetic task (see Figure 1). Commonly, an alternative indirect strategy, which consists of a two-step alkylation/oxidation protocol, involving 4,7-dihydroindoles as Friedel–Crafts partners, is used for this purpose.[5]

In contrast, the stereoselective functionalization of indoles at the N1 position, which would represent a valuable shortcut to numerous enantiomerically pure natural tricyclic indolyl alkaloids (e.g., Mitomycins[6] and indolocarbazoles[7]) is still mostly unexplored. Only a few examples have been reported so far: chiral Pd (Trost)[8a,b] and Ir (Hartwig)[8c] complexes have been found to assist the chemo-, regio-, and stereoselective N-allylic alkylation of indoles, and very re-

[a] Dr. M. Bandini, Prof. A. Bottoni, Dr. A. Eichholzer, Dr. G. P. Miscione
Dipartimento di Chimica "G. Ciamician"
Alma Mater Studiorum—Università di Bologna
via Selmi 2, 40126 (Italy)
Fax: (+39) 51-2099456
E-mail: marco.bandini@unibo.it
gianpietro.miscione@unibo.it

[b] Dr. M. Stenta
Laboratory for Biomolecular Modeling
Ecole Polytechnique Fédérale de Lausanne (EPFL)
1015 Lausanne (CH)

Supporting information for this article is available on the WWW under http://dx.doi.org/10.1002/chem.201000560.

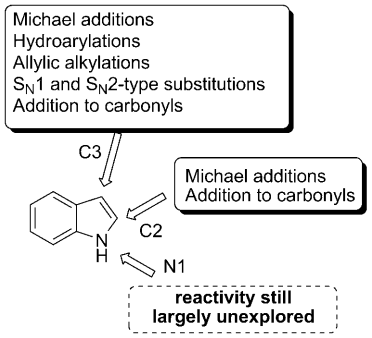

Figure 1. Catalytic enantioselective routes to functionalized indolyl cores. Regioselective N1-alkyaltion is still a synthetic challenge.

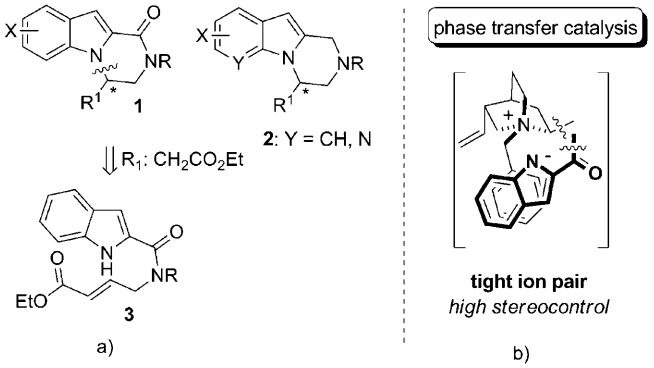

Figure 2. a) General formula structures of 3,4-dihydropyrazino[1,2-*a*]indol-1(2*H*)-ones (**1**) and 1,2,3,4-tetrahydropyrazino[1,2-*a*]indoles (**2**). b) Pictorial representation of the postulated contact ion pair between chiral quaternary ammonium salts and indolinate intermediate in the PTC enantioselective intramolecular N-alkylation of indoles.

cently Chen[9a] and Enders[9b] have demonstrated the efficiency of chiral organocatalysis in the stereoselective indole N1 functionalization through Morita–Baylis–Hillman reactions and domino aza-Michael/aldol condensation reactions, respectively.

As a part of our continuing effort at developing new catalytic and enantioselective procedures for the "decoration" of indolyl cores,[2f,10] we have recently addressed the challenging N1 alkylation reaction based on the use of intramolecular aza-Michael addition.[11] The main goal of the protocol was the preparation of active pharmaceutical ingredients (APIs), such as functionalized 3,4-dihydropyrazino[1,2-*a*]indol-1(2*H*)-ones (**1**), which have recently attracted attention as specific inhibitors of serotonergic receptors and for their noncompetitive antihistamine activity (Figure 2a).[12] Moreover, structurally correlated 1,2,3,4-tetrahydropyrazino-[1,2-*a*]indoles (**2**) have risen to prominence as effective medicinal additives for anti-obesity, and in the treatment of non-insulin-dependent diabetes.[13] Notably, the direct synthetic access to such a class of compounds in enantiomerically pure form is still a demanding task, and the existing methodologies typically require crucial preparative steps, such as the resolution of racemates or the use of chiral auxiliaries/chiral pool.[13,14]

Our working hypothesis deals with the direct construction of **1** through a stereoselective intramolecular C–N bond-forming process, exploiting the preferential N1-site reactivity when electron-withdrawing groups (EWGs) are present at both C2 and C3 indole positions.[9] In particular, based on our recent findings on the K_2CO_3-catalyzed synthesis of functionalized pyrazino-indolinones (**1** with $R^1 = CH_2CO_2Et$),[15] we envisioned that intramolecular aza-Michael addition, under phase-transfer-catalysis (PTC)[16] conditions, could ensure the formation of sufficiently tight ion pairs between the chiral ammonium salt and the indolate intermediate (obtained from **3**) to provide efficient stereodiscrimination. A schematic representation of the hypothetical tight ion pair, with a portion of quaternary ammonium salt deriving from *Cinchona* alkaloids, is given in Figure 2b. It is worth pointing out that, despite the impressive synthetic potential for the preparation of nitrogen-containing heterocycles, the catalytic and enantioselective intramolecular aza-Michael addition still remains quite an unexplored field.[17]

After a severe optimization phase, we were delighted to find out that *N*-benzylcinchonidinium bromide **4a** (10 mol%), carrying a strong EWG (e.g., CF_3) in the *para* position of the benzyl substituent, proved to be an effective catalyst for the ring-closing event. The phase-transfer regime (toluene, KOH_{aq}, −45 °C) led to (*S*)-**1a** in 93% yield and 91% enantiomeric excess (Scheme 1).

The reaction scope was then promptly studied. Wide tolerance towards electron-deficient and electron-donating

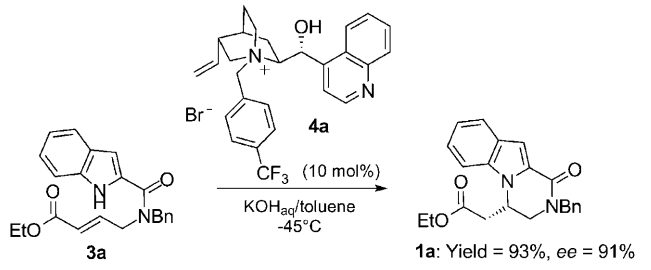

Scheme 1. Optimal reaction conditions for the PTC asymmetric synthesis of pyrazinoindolone **1a**.

Abstract in Italian: *La catalisi asimmetrica per trasferimento di fase è, a tutt'oggi, una fra i metodi di sintesi stereoselettivi più efficaci per la preparazione di intermedi chiave dell'indotto farmaceutico. Tuttavia, i complessi network di legami deboli che generalmente si instaurano fra catalizzatore e substrato in queste trasformazioni non consentono di comprendere appieno gli aspetti alla base delle elevate stereoselezioni ottenute. In questo studio, con un approccio combinato sperimentale/computazionale, vengono esplicitati gli aspetti meccanicistici chiave nella sintesi enantioselettiva di composti ad elevato valore aggiunto come i diidro-pirazinoindoloni, tramite addizione tipo aza-Michael intramolecolare per trasferimento di fase (IMAMR).*

substituents on the indolyl ring was recorded, thus providing direct access to a library of indolinones **1** in high yields and with excellent enantiomeric excesses. A representative collection of tricyclic compounds (**1b–g**) is reported in Scheme 2.

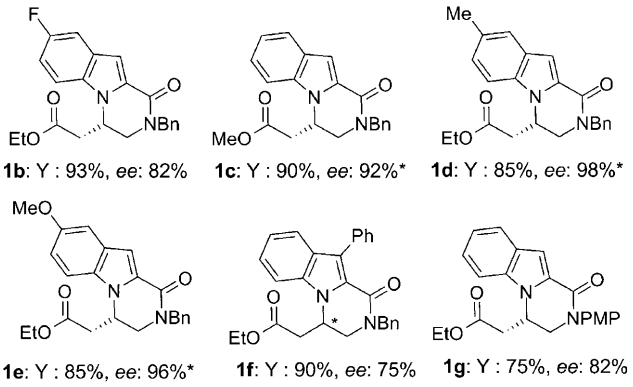

Scheme 2. Enantiomerically enriched dihydro-pyrazinoindolinones synthesized through asymmetric PTC (PMP: *para*-methoxyphenyl; *: after recrystallization).

It has been frequently observed that *Cinchona* mediated, asymmetric phase-transfer catalysis deals with chemical and optical outcomes which are strongly related to the structural decoration of the chiral ammonium salts at the C9 position, at the C6′ position of the quinoline ring, and the benzyl framework (Figure 3). This aspect has generally caused frustrating and time-consuming trial-and-error approaches for discovering optimal conditions, because of the large number of structural variables to be taken into account. Within this context, a reliable model providing a rationale of the network of weak, nonbonded catalyst–substrate interactions responsible for the enantiodiscriminating event would dramatically enhance the synthetic feasibility of such a class of processes in the total synthesis of natural products and large-scale productions by shortening the optimization phase.

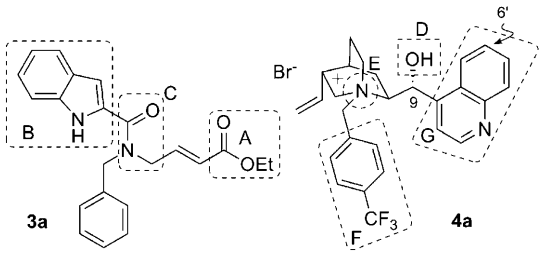

Figure 3. Crucial binding sites of substrate and *Cinchona* derivative acting as a catalyst.

Despite the extent of chiral *Cinchona* ammonium salts in asymmetric phase-transfer catalysis, and the enormous efforts devoted to elucidating its mechanism of action (mainly concerning alkylation processes),[18] very few examples describing intramolecular processes have been reported so far. Prompted by such a task, we present here a full account on the PTC asymmetric aza-Michael alkylation of indoles. In particular, we carry out a combined experimental and theoretical investigation of the reaction reported in Scheme 1, in which we selectively introduce specific structural variations in the substrate and catalyst, with the aim of gaining an insight into the mechanistic aspects of this process.

Results and Discussion

The hypothetical mechanism of the PTC intramolecular N1-indole alkylation can be thought to involve three main events. Initially, the indolyl ester **3** is deprotonated by OH^- ions provided by the external inorganic species (presumably at the interfacial region), and the resulting reactive indolinate intermediate is intercepted by the chiral quaternary ammonium salt. The well-constructed structure of the *Cinchona* alkaloid provides the electronic and steric constraints that favor a proper folding of the acyclic precursor **3** to reach a structural arrangement in which the nucleophilic (indole nitrogen atom) and electrophilic (β-carbon atom of the ester moiety) centers are spatially close. It is plausible to believe that a network of electronic interactions between the substrate and the peripheral catalyst substituents work simultaneously to stabilize the ring-closing transition state (TS) with synchronized control of the stereochemistry of the process. Finally, the negatively charged enolate intermediate is rapidly neutralized by the proton originating from the re-aromatization of the indole nucleus, leading to the final cyclic product **1**, which is released in solution.

The crucial phase for the actual overall transfer of chirality from the catalyst to the final pyrazinoindolone should be represented by the formation of conformationally rigid and stereochemically defined **3a**–**4a** ion pair resulting from a network of complementary attractive interactions between catalyst and substrate. Within this conceptual model, the ester moiety (A), the indole ring (B), and the amide group (C) should represent crucial binding sites of the substrate (see Figure 3). On the other hand, it is conceivable that the *Cinchona* derivative preferentially interacts with the precursor **3a** through the hydroxyl group (a potential source of hydrogen bonds) at the C9 position (D), the positively charged quinuclidine nitrogen atom (E), the benzyl group bonded to nitrogen (F), and the quinoline ring (G).

With this model in mind, we have carefully investigated the potential-energy surface (PES) for the complexes that originate from the interaction and binding of the deprotonated model substrate **3c** with the catalyst **4a** (Scheme 1). The key factors that differentiate the possible resulting adducts are the weak "complementary" interactions that engage the various groups of substrate (A, B, and C) and catalyst (D, F, and G) as previously shown in Figure 3. Most of these attracting "contacts" are parallel or T-shaped π-stacking interactions involving the various π systems of both molecules. An additional important interaction should be

the effective hydrogen bond that can be established between the free hydroxyl group (D) bonded at the C9 position of the catalyst and the substrate carbonyl groups of the ester (C) or the amide group (A).

Among the various catalyst–substrate adducts located on the PES, one special type of structural arrangement has been found to be more stable than the others. This particular arrangement characterizes the two conformationally rigid isomers **M1-S** and **M1-R**, which represent the starting complexes for the two reaction channels leading to the (*S*)-**1c** and (*R*)-**1c** products, respectively. A schematic representation of the two structures is given in Figure 4, in which a set of important geometrical parameters is also reported. One point concerning these drawings should be stressed here. Because, in addition to a conventional three-dimensional picture (bottom part of Figure 4) we have also adopted a two-dimensional representation, in this latter case several atomic distances are not realistic and appear much longer (or shorter) than in the real molecule. A comparison to the more realistic three-dimensional picture reported in the same figure should help to comprehend the relative positions of the various groups. A further point that must be mentioned concerns the numbering of the various atoms: in the following discussion we have replaced the separated notations for substrate and catalyst (previously used) with a global notation (reported in the figure) for the whole substrate–catalyst adduct. Furthermore, for the sake of simplicity, we have indicated only the atoms explicitly considered in the discussion.

It is important to stress some structural features of **M1-S** and **M1-R.** In both structures, the two atoms involved in the formation of the new C–N bond (e.g., the formally negative nitrogen atom N2 and the electrophilic C2 carbon atom of the α,β-unsaturated ester group) are facing each other, and, thus, they already point in a suitable direction for the nucleophilic attack to take place. Isomers **M1-S** and **M1-R** differ mainly in the orientation of the ester moiety. Interestingly, the two species are conformational isomers which can interconvert by a simple rotation around the C1–C2 bond, thus exposing one or other of the two ester pro-chiral faces to the attack of the nucleophilic nitrogen N2.

We consider first in detail the structural features of the more stable isomer **M1-S**, affording the (*S*)-**1c** enantiomeric product (C2–N2 distance for the new forming bond = 3.021 Å). The main force driving the substrate and catalyst together is electrostatic in nature. Two opposite charges are located on the former (negative) and latter (positive) species. Even if the two charges are formally located on N2 and N3, the computational results clearly show that they are strongly delocalized. The real (computed) net charge on N2 is −0.58, but significant negative charges are also present on O1 and O3: −0.61 and −0.63, respectively. Furthermore, the actual computed net charge on N3 is +0.57, but other atoms of the catalyst belonging to the quinoline ring bear a significant positive charge: +0.86 on C8 and +0.70 on C7. Additional attractive interactions between substrate and catalyst are evident in **M1-S**. First of all, as previously suggested, a strong hydrogen bond involves H1 (D hydroxyl group

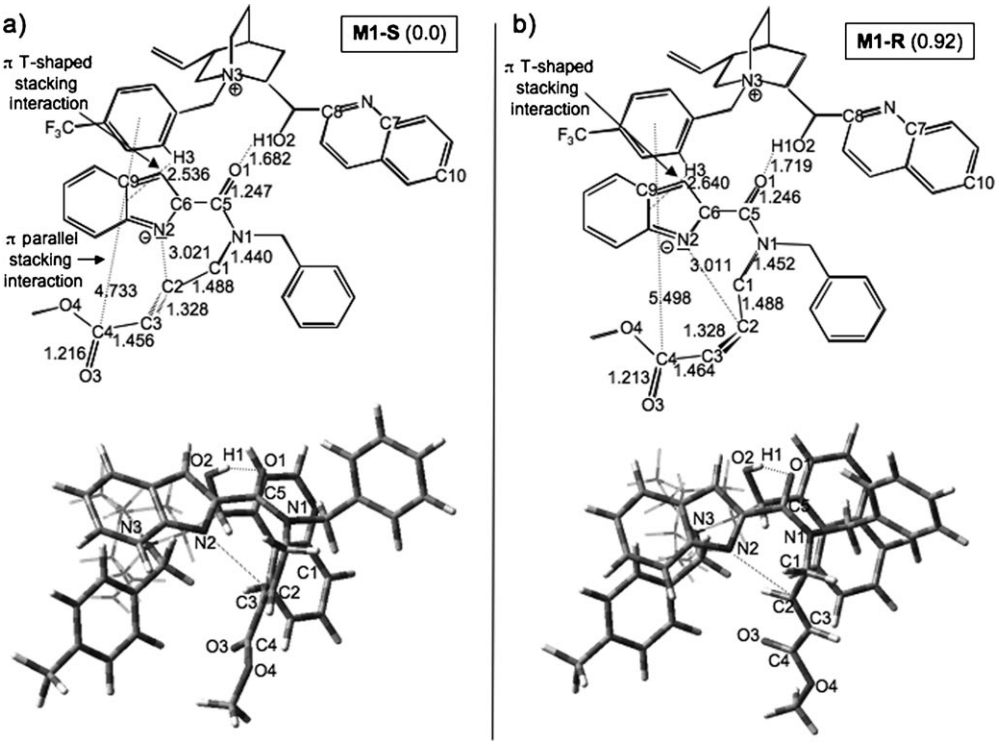

Figure 4. A schematic representation of **M1-S** and **M1-R** in two and three dimensions. Bond lengths are in Å. When not connecting atoms, dashed lines connect the ring centroids.

O2H1) and O1 (carbonyl oxygen), as evidenced by the short H1···O1 distance (1.682 Å) and the lengthening of the C5–O1 carbonyl bond (1.247 Å). The crucial role of the hydroxyl group of **4a** in tightening the catalyst/indolinate ion pair has also been demonstrated experimentally. For instance, the model reaction, in which C–OH was replaced by C-O-allyl in **4a**, afforded **1a** in good yield (85%) but in nearly racemic form (*ee* = 5%). Two π-stacking interactions (both engaging the catalyst electron-poor benzyl–CF_3 ring) contribute to bind the substrate and catalyst in a rigid conformation. One of the two interactions is π T-shaped and involves the catalyst benzyl–CF_3 group and the substrate indole ring. The second interaction is a weaker parallel π-stacking interaction occurring between the catalyst benzyl–CF_3 group and the substrate ester π system, which lie on parallel planes. As a matter of fact both interactions are neither perfect T-shaped nor parallel π-stacking interactions. A slightly oblique relative assembly of the interacting groups is evident from our computations, and this allows the benzyl–CF_3 ring to interact with both partners. A series of test calculations on a simpler model system (see Figure S1 of the Supporting Information) has shown that a perfect T-shaped interaction between the benzyl–CF_3 ring and the indole systems would be highly favored. However, such a perfect T-shaped arrangement is not actually observed in the real system due to steric hindrance, and because it would not allow the additional interaction between the benzyl–CF_3 ring and the ester. Additional calculations have demonstrated that a different orientation of the benzyl group bonded to N1, and resulting in a π-stacking interaction with quinoline, is less stable than the one actually observed, for which the N1-benzyl ring rotates and moves far away from the quinoline group. It is evident that, when quinoline and the N1-benzyl are spatially close, the presence of the benzyl ring causes a steric perturbation on the conjugation of the planar N2-C6-C5-N1-C1 system. Thus, a conformation in which this conjugation is preserved is favored at the expense of the loss of the benzyl–quinoline interaction.

The conformer **M1-R** lies 0.92 kcal mol^{-1} higher in energy than **M1-S**. Analysis of the various interactions can provide a rationale for this energy gap. Firstly, the H1···O1 hydrogen bond is weaker in **M1-R** than in **M1-S** (the H1···O1 distances are 1.719 and 1.682 Å, respectively). Also, the π-stacking interaction between the benzyl–CF_3 group and the indole rings becomes weaker. This is evidenced by the lengthening of the distance between H3 and the centroid of the six-membered ring of the indole fragment (2.640 and 2.536 Å in **M1-R** and **M1-S**, respectively). Finally, in **M1-R**, the interaction between the substrate ester group and the catalyst benzyl–CF_3 fragment is absent, because the two groups are now too distant. These structural features are a direct consequence of the different orientation of the ester moiety in the two isomers. Whereas in **M1-S** the C1-C2-C3-C4 plane is almost perfectly orthogonal to the C1-N2-C5-C6-indole system plane (the dihedral angle N1-C1-C2-C3 is 2°), in **M1-R**, the ester is bent away from the benzyl–CF_3 ring (the dihedral angle N1-C1-C2-C3 becomes 117°).

Now the following question arises: why is the ester chain bent in **M1-R** even if this arrangement results in an overall destabilization? An explanation can be found by analyzing the structure of the aminopropene unit N1-C1-C2-C3. It is known that in propene the eclipsed conformation is more stable than the staggered one. This can easily be explained by the change of orbital interactions between the two out-of-plane methyl hydrogen atoms and the double-bond π system on passing from the staggered to the eclipsed conformer.[19] In agreement with this structural preference, in both **M1-S** and **M1-R** adducts the aminopropene unit adopts an eclipsed conformation (i.e. the C1–N1 bond is eclipsing the C2=C3 double bond). However, in **M1-R** this moves the ester chain far away from the benzyl–CF_3 ring, thus preventing any stabilizing π-stacking interaction. Thus, the more stable eclipsed conformation of the aminopropenic unit contributes in turn to the lower stability of **M1-R** with respect to **M1-S**. The relative position of the C1–N1 and C2–C3 bonds is evident in the three-dimensional representation of Figure 4. However, for a better understanding of the aminopropene fragment structural features, a more detailed representation is given in Figure S2 of the Supporting Information.

A conformational transition state (rotation around the C1–C2 bond) connecting the two isomers **M1-S** and **M1-R** has been located (see Figure S3 in the Supporting Information). The two barriers (2.27 and 1.35 kcal mol^{-1} considering **M1-S** and **M1-R,** respectively, as the starting point) are consistent with the rotational barrier values usually found for single bonds. These values show that the interconversion between the two minima is a rather easy process.

Other possible conformers that can be obtained from **M1-S** and **M1-R** have been examined. In particular, rotation around the C3–C4 bond has been considered in both species. Specifically, we have located a conformer (obtained from **M1-R)** in which the ester chain is twisted towards the benzyl–CF_3 fragment. However, in all cases examined here, the new structures are higher in energy with respect to **M1-S** and **M1-R**. Thus, all the possible reaction paths stemming from these additional initial adducts are quite unlikely, and will not be discussed in the following.

A transition state describing the C2–N2 bond formation and the consequent ring closure has been found along both reaction paths (originating from **M1-S** and **M1-R**). The two transition states are **TS1-S** and **TS1-R**, and lead to the (*S*)-**1c** and (*R*)-**1c** products, respectively (Figure 5). Transition state **TS1-S** is 5.73 kcal mol^{-1} higher than the preceding complex **M1-S** (intrinsic activation barrier). The formation of the new C2–N2 bond (bond length = 2.003 Å) following the nucleophilic attack causes a shifting of the electronic density along the C2-C3-C4-O3 framework and a consequent change in character of the three bonds. In particular, the single-bond character of C2–C3 (1.373 Å) and C4–O3 (1.229 Å) increases, whereas C3–C4 (1.421 Å) is turning into a double bond. The strength of the important intermolecular O1···H1 hydrogen bond does not change too much, the O1···H1 distance being only 0.019 Å longer with respect

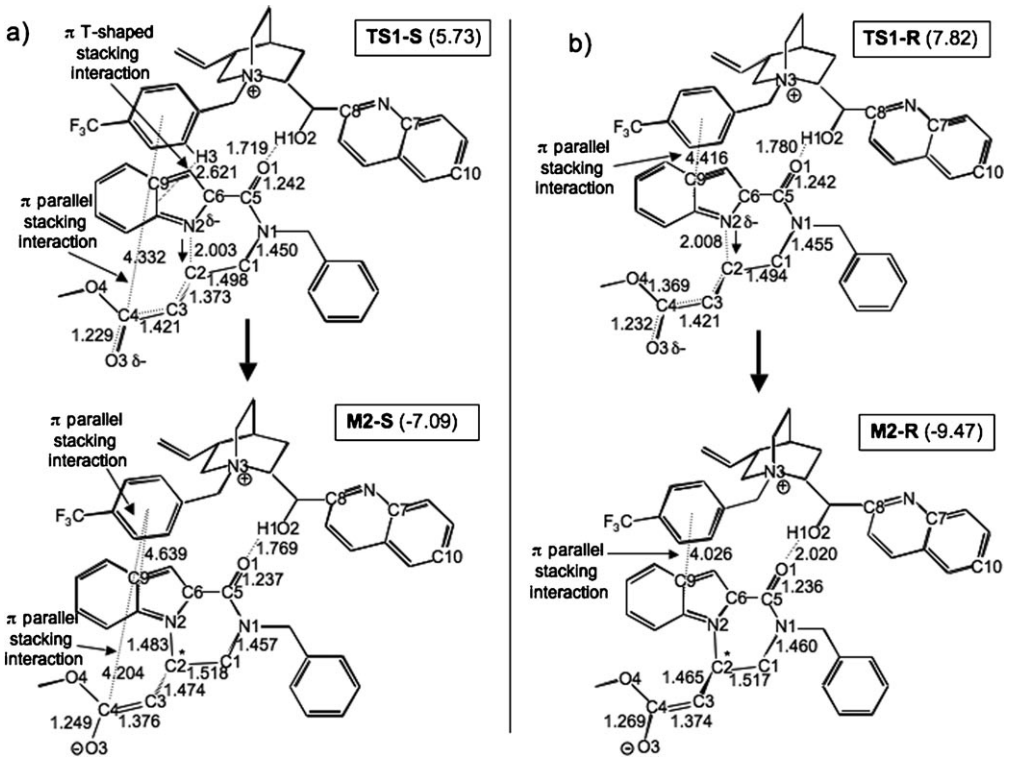

Figure 5. A schematic representation of the two transition states **TS1-S** and **TS1-R** and the corresponding product adducts **M2-S** and **M2-R.** Bond lengths are in Å. When not connecting atoms, dashed lines connect the ring centroids.

to **M1-S**. Because in this transition structure the ester chain is twisting toward the indole moiety, it moves nearer to the benzyl–CF_3 fragment, and the relative π-stacking interactions become stronger. This is evidenced by the variation of the distances between the centroid of the benzene ring and the two atoms C4 and O4 on passing from **M1-S** to **TS1-S**. These parameters decrease from 4.733 and 5.058 Å to 4.332 and 4.203 Å, respectively.

The computed activation energy for **TS1-R** (along the alternative (*R*)-**1c** pathway) is 6.90 kcal mol^{-1}, and, importantly, **TS1-R** is 2.09 kcal mol^{-1} higher in energy than **TS1-S**. The length of the new forming bond C2–N2 (2.008 Å) varies only slightly with respect to **TS1-S**. In contrast, the intermolecular H1···O1 distance becomes longer (1.780 Å) than in **TS1-S**, indicating a weakening of this relevant interaction.

Two important structural differences are evident in the comparison between **TS1-S** and **TS1-R**: these are the inner conformation of the ester chain and the relative position of the indole and benzyl–CF_3 aromatic systems. In **TS1-R**, the direction of the ester chain allows N2 and C2 to reach suitable relative positions for the formation of the new bond, but forces the aminopropene framework (N1-C1-C2-C3) to adopt a less stable staggered conformation. As a consequence, the ester moiety cannot be properly oriented for an effective π-stacking interaction with the benzyl–CF_3 fragment. At the same time, to avoid destabilizing steric interactions, the benzyl–CF_3 ring must rotate, and its plane becomes almost parallel to the indole plane. This structural change transforms the indole-benzyl T-shaped π interaction that characterizes **TS1-S** into a less stabilizing parallel π interaction in **TS1-R** (compare **TS1-S** and **TS1-R** in Figure 5). As mentioned above, calculations on simpler model systems, for which only the π systems of the indole and benzyl–CF_3 groups are considered, clearly show that a T-shaped π interaction is more stable than a parallel one, and, when steric hindrance can be neglected, this represents the preferred arrangement. In summary, our analysis indicates that the higher energy of **TS1-R** with respect to **TS1-S** is caused by: 1) a weaker O1···H1 interaction; 2) the unfavorable conformation of the amino-propene unit; 3) the lack of π-stacking interactions involving the ester moiety; and 4) the different and less favorable relative orientation of the indole and benzyl–CF_3 groups.

TS1-S and **TS1-R** lead to the product adducts **M2-S** and **M2-R**, respectively (bottom sections of Figure 5a and b). The two structures, characterized by the six-membered cycle C1-N1-C5-C6-N2-C2, are epimers, which differ in their configuration at the C2 center. In both cases, the cycle adopts a half-chair-like conformation, where C1, N1, C5, C6, and N2 are coplanar and C2 is bent out of the plane. In **M2-S** the unsaturated chain is pseudo-axial, whereas it becomes pseudo-equatorial in **M2-R**. Even if the negative charge is now formally located on O3, the C2–C3, C3–C4 and C4–O3 bond lengths clearly indicate a strong delocalization: C3–C4 is longer than a double bond (1.376 Å in **M2-S** and 1.374 Å in **M2-R**), whereas C2–C3 (1.474 Å in **M2-S** and 1.465 Å in **M2-R**) and C4–O4 (1.249 Å in **M2-S** and 1.269 Å in **M2-R**) are shorter than normal single bonds. In **M2-S** the ester

chain is slightly twisted towards the benzyl–CF_3 fragment. This arrangement gives rise only to a weak π-stacking interaction, which is not possible in **M2-R**, where (as noted in **TS1-R**) the benzyl and indole planes are parallel and the ester moiety is not involved in any π-stacking interaction.

The energy profile of the reaction, which is exothermic (the product **M2-S** is 7.09 kcal mol^{-1} lower than **M1-S**) is reported in Figure 6. It is interesting to note that the relative stability of the two product adducts is reversed with respect to that of the corresponding reagents and transition states, **M2-R** being 2.38 kcal mol^{-1} more stable than **M2-S**. This finding cannot be ascribed to the O1···H1 hydrogen bond, because the O1···H1 distance increases on going from transition states to products, but remains significantly shorter in **M2-S** (1.769 Å) than in **M2-R** (2.020 Å). It is plausible that an important contribution to the greater stability of **M2-R** is represented by the pseudo-equatorial orientation of the ester substituent in the cycle.

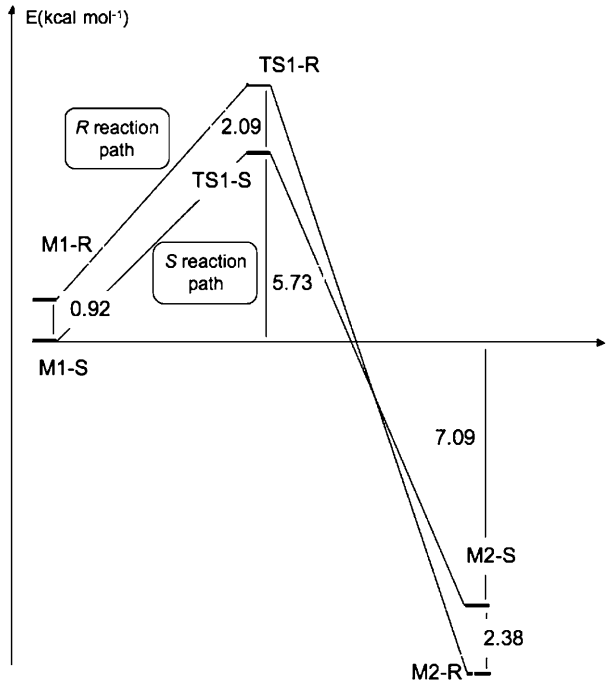

Figure 6. Computed reaction energy profile.

We now compare the computed energy profile to the experimental evidence. Because the reaction is carried out under kinetic conditions (at a temperature of −45 °C), to evaluate the ratio between the two possible products (and ultimately the reaction *ee*) we do not have to consider their relative stability, which would erroneously indicate the *R* isomer as the favored product. As the barrier for the conformational interconversion between the two starting complexes is significantly lower (2.31 kcal mol^{-1} for the **M1-S**→**M1-R** conversion) than that required by the ring-closing process (5.73 kcal mol^{-1} for the **M1-S**→**TS1-S** transformation), following the Curtin–Hammet principle, the ratio between the two products is determined by the energy difference between the corresponding transition states **TS1-R** and **TS1-S**. This difference is equal to 2.09 kcal mol^{-1}, and at −45 °C this value corresponds to a ratio **M2-S**:**M2-R** of approximately 99:1. This would lead to a 98 % *ee*, which is in good agreement with the experimentally observed value of 90 %.

To reveal the effects of the catalyst we have carried out additional computations on the sole substrate (uncatalyzed reaction). The results can be summarized as follows: a) the two starting isomers are very close in energy, their energy difference being only 0.31 kcal mol^{-1} (with the *R* isomer favored); b) the two transition states become almost degenerate because their energy gap drops from 2.09 kcal mol^{-1} to 0.03 kcal mol^{-1}. Thus, it is evident that the catalyst inclusion (and its interaction with the substrate) is essential for differentiating the two diastereomeric pathways.

The role of the catalyst–substrate interactions has been further investigated by means of new calculations on "mutated" complexes. To this purpose we have considered the model substrate **3h** (Scheme 3) in which the amide benzyl

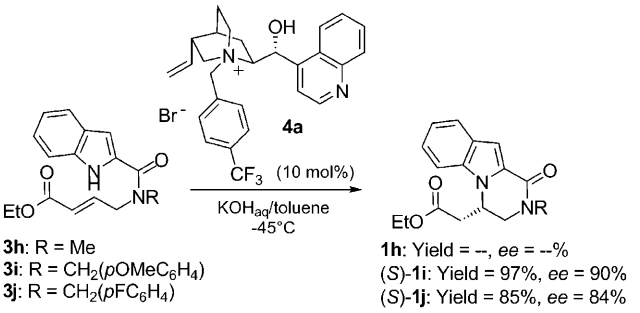

Scheme 3. Proving the effect of the amide substituents on the course of the asymmetric cyclization.

fragment has been replaced by a methyl group. We have found that, after optimization, the energy difference between the two starting complexes **M3-S** and **M3-R** (Figure S4 in the Supporting Information) is 0.79 kcal mol^{-1} with **M3-S** favored (thus, very close to the value of 0.92 kcal mol^{-1} found for **M1-S** and **M1-R**). Our computations show that the O1···H1 hydrogen bond becomes weaker on passing from **M3-S** to **M3-R** (the H1···O1 distance is 0.130 Å longer in the latter case). However, in **M3-R**, as the cumbersome benzyl group is lacking, the quinoline can approach the ester group to give rise to a T-shaped π-stacking interaction. The structural features indicate that this interaction is weaker in **M3-S** and, thus, can partly balance the reduced strength of the O1···H1 hydrogen bond. The computations carried out on the transition states **TS2-R** and **TS2-S** along the two reaction pathways originating from **M3-R** and **M3-S**, respectively, show that their energy difference (2.10 kcal mol^{-1}) is nearly identical to the value found for **TS1-R** and **TS1-S**, and the *S* pathway is still favored. This finding is in agreement with the evidence that the benzyl group did not

concur substantially with the catalyst–model substrate aggregation, and, consequently, to the differentiation of the two reaction channels.

To validate this theoretical model, the compound (*E*)-ethyl-4-(*N*-methyl-1H-indole-2-carboxamido)but-2-enoate **3h** was synthesized and subjected to IMAMR under optimal conditions. However, the poor solubility of **3h** prevented the catalytic process from taking place (Scheme 3). Therefore, acyclic precursors bearing benzyl groups with electron-donating and electron-withdrawing substituents (e.g. **3i,j**) were readily prepared and allowed to cyclize in the presence of **4a** (10 mol%) in toluene at −45 °C. The corresponding pyrazinoindolones **1i,j** were isolated with similar chemical and optical yields (*ee* = 84–90%). These results, together with the case reported above for **1g** (R = PMP, Scheme 2, *ee* = 82%) supports the previously described computational outcomes underlying marginal importance of the amide substituent (Scheme 3) on the overall chemical course.

In contrast, the amide moiety in **3** exerts a significant influence on the overall catalytic reaction. This has been theoretically and experimentally verified by taking into account the indolyl-ester **3k** (Scheme 4), which was directly obtained

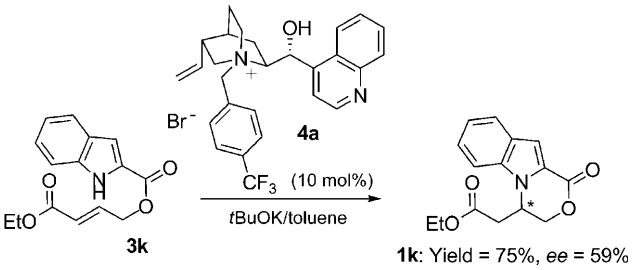

Scheme 4. Asymmetric phase-transfer-catalyzed aza-Michael addition of indolyl-ester **3k**.

in unoptimized 25% yield through condensation of indole-2-carboxylic acid and ethyl 4-bromocrotonate under basic conditions (see Supporting Information). In this case, the replacement of the nitrogen N1 with the oxygen O5 is expected to cause a decrease of the electron density on the substrate carbonyl oxygen O1. To validate the effect of this substrate "mutation" we have optimized the structures of the new adducts **M4-S** and **M4-R** obtained by replacing the substrate N1-benzyl unit with an oxygen atom. The energy difference between the two complexes **M4-S** and **M4-R (**see Figure S5 of the Supporting Information) is 1.77 kcal mol^{-1} with the *S* isomer favored. It is interesting to notice the significant lengthening of the O1···H1 distance (about 0.15 Å) with respect to **M3-S** and **M3-R** (from 1.666 to 1.704 Å and from 1.796 to 1.852 Å, respectively). This finding clearly demonstrates that the O1···H1 hydrogen bond is significantly stronger when an amidic carbonyl is involved. The decrease of the energetic contribution of the O1···H1 interaction is also in agreement with the stabilization energy computed for **M4-S** with respect to the isolated catalyst and substrate, which is about 2 kcal mol^{-1} lower than the value computed for **M1-S** (89.60 and 91.29 kcal mol^{-1}, respectively). The two corresponding transition states, **TS3-S** and **TS3-R** (also depicted in Figure S5), are almost degenerate in energy, **TS3-R** being only 0.16 kcal mol^{-1} lower than **TS3-S**. This computational outcome is in agreement with the moderate stereoselection (*ee* = 59%, see Scheme 4) observed experimentally. The reduced energy gap between the two transition states is a direct consequence of the replacement of an amide group by an ester group. Because the conjugation in the N2-C6-C5-O-C1 system becomes poorer, the oxygen is now placed out of the N2-C6-C5 plane. Especially in **TS3-R**, this allows the ester chain to adopt a different conformation that minimizes the steric repulsion with the benzyl–CF_3 ring, which, in turn, can establish a stronger key π-stacking interaction with the indole fragment with respect to the corresponding structures with the amide group. This structural change in the substrate also determines a lengthening of the O1···H1 hydrogen bond with respect to the reference transition states **TS1-S** and **TS1-R** (from 1.719 Å to 1.754 Å in the *S* structures and from 1.780 Å to 1.920 Å in the *R* structures). This indicates that in **TS3-R** it is more convenient for the system to weaken the hydrogen bond strength in order to maximize the above-mentioned π-stacking interactions. In contrast, the π-stacking interactions between the benzyl–CF_3 group and the terminal ester moiety are not significantly affected: the distance between C4 and the centroid of benzyl–CF_3 is 4.332 Å in **TS1-S** and 4.278 Å in **TS3-S**.

In addition to the effect of the weaker O1···H1 hydrogen bond described previously, it is worth outlining the less pronounced propensity of the ester moiety (with respect to its amidic counterpart) to fold the acyclic precursor **3k** to reach the optimal geometry for the ring-closing process. This factor certainly contributes to the lower reactivity of **3k** with respect to **3i** and **3j**. In this case, an appreciable isolated yield (75%) (in addition to the moderate *ee* (59%) previously mentioned) was obtained using a stoichiometric amount of *t*BuOK as a base in toluene at room temperature (Scheme 4). Attempts to improve the level of stereodiscrimination by lowering the reaction temperature failed, causing an unacceptable drop in the reaction rate with no significant variations on the final optical yield.

Additional computations have been performed on modified model systems in which we have replaced the methyl group on the ester chain with a *tert*-butyl group characterized by greater steric hindrance. The presence of the more cumbersome ester substituent is responsible for a steric perturbation that destabilizes the *S* structures more, both in the two starting adducts **M5-S** and **M5-R** (see Figure S6 in the Supporting Information) and in the two transition structures. As a matter of fact, the energy differences between **M5-S** and **M5-R** (0.79 kcal mol^{-1}) and between the two related transition states **TS4-S** and **TS4-R** (1.67 kcal mol^{-1}) decrease. The bulky *tert*-butyl group introduces a more evident steric perturbation with the benzyl–CF_3 ring in the *S* structures, and also causes a weakening of the parallel π-stacking interaction between the catalyst benzyl–CF_3 group and the substrate ester π system, which is present in the *S* structures

only. The two intrinsic activation barriers are rather similar (7.62 and 8.32 kcal mol^{-1} for the *S* and *R* path, respectively), and are in both cases larger than in the reference model system with the ester methyl group. These computational data are in rather good agreement with the experimentally observed decrease of the reaction yield and of the enantiomeric excess (yield: 90%→61%, *ee*: 90%→53%). Besides the importance of the O1···H1 hydrogen bond, the trend of the previously described π-stacking interactions between the indolyl ring and the benzyl substituent of the quinuclidine nitrogen atom seems to match the reported experimental data satisfactorily. In particular, it has been found that: 1) EWGs favor the discriminating T-shaped π interactions (e.g., *p*-F, *p*-NO_2 and *p*-benzyl–CF_3 substituents lead to comparable results); and 2) a *para* substitution pattern of the benzyl unit is strictly required, as the introduction of groups in the *meta* and/or *ortho* positions (e.g., F, NO_2, 9-anthryl) causes an important decrease in the enantiomeric excess.

In principle, the T-shaped interactions should become much less important if we reduce the extension of the interacting π-electron clouds. This would be the case of pyrrole-analogous **3l** and **3m**, which, after a survey of chiral alkaloid-derived quaternary ammonium salts **4b–d** (Scheme 5), led to the synthetically useful 1,2,3,4-tetrahydropyrrolo[1,2-*a*]pyrazinones **1l** and **1m** in high yield but lower enantiomeric excess up to 56% (Table 1).

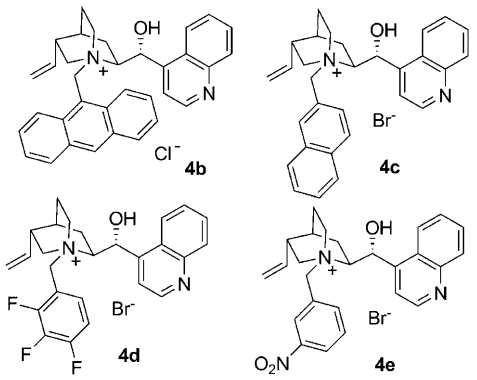

Scheme 5. Set of chiral ammonium quaternary salts **4b–e** used in the PTC intramolecular N-alkylation of pyrrolyl derivatives.

These points have been validated by further computations, showing that in both adducts **M6-S** and **M6-R** (emulating the pyrrole-analogous **3l** and **3m**) no interactions between the pyrrolyl group and the benzyl–CF_3 fragment are evident (see Figure 7). The π systems of the two groups are in this case too far away to give rise to an effective interaction. On the other hand, to force them to stay closer would cause a weakening of the strong H1···O1 hydrogen bond, which, on the contrary, becomes stronger in **M6-S** (1.643 Å) and **M6-R** (1.685 Å) with respect to **M1-S** (1.682 Å) and **M1-R** (1.719 Å), respectively.

Our computations show a significant decrease of the energy difference between the two diastereomeric pathways.

Table 1. Asymmetric PTC aza-Michael addition of pyrrolyl ester **3l** and **3m**.[a]

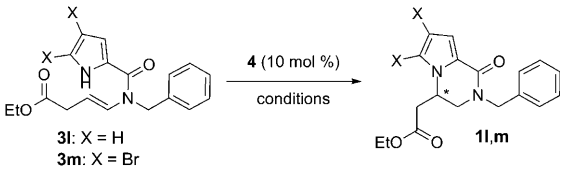

3l: X = H
3m: X = Br

Entry	3	4	Conditions[b]	Yield [%][c]	*ee* [%][d]
1	**3l**	**4a**	A	82	54
2	**3l**	**4b**	A	–	–
3	**3l**	**4b**	B	88	18
4	**3l**	**4c**	B	79	30
5	**3l**	**4c**	A	75	29
6	**3l**	**4d**	B	85	13
7	**3l**	**4e**	A	80[e]	31
8	**3m**	**4a**	A	77	56

[a] All the reactions were carried out in reagent grade toluene without any moisture restriction. [b] A: KOH_{aq} (25%, 0.5 equiv), −45 °C, 16 h; B: KOH_{aq} (25%, 0.5 equiv), RT, 16 h. [c] Yields after flash chromatography. [d] Determined by HPLC on a chiral stationary phase. [e] After 48 h.

In particular, **M6-S** is only 0.14 kcal mol^{-1} more stable than **M6-R**, and the two corresponding transition states also are very close in energy, **TS5-R** being only 0.35 kcal mol^{-1} more stable than **TS5-S**. It is therefore evident that the interactions involving the phenyl moiety of the indole ring and the benzyl–CF_3 group are crucial for determining the stereochemical outcome of the reaction. Even in this case, the computational evidence is in good agreement with the experimental outcome, showing only moderate stereoselection (*ee* = 54–56%), and indicates that the indole system is essential in determining the enantioselective character of the process.

Conclusion

In this paper a full account addressing the stereoselective N1-alkylation of indoles through intramolecular phase-transfer catalysis has been presented. In particular, combined computational (DFT) and experimental investigations have been carried out to understand how chiral *Cinchona* quaternary ammonium salts exert perfect stereodiscrimination in the ring-closing event. The computational results have demonstrated that a complex network of single- and multi-point nonbonded catalyst/substrate interactions is responsible for the observed stereoselection.

We have considered as a reference model system the adducts formed by the substrate **3c** and the catalyst ammonium salt **4a**. Because the reaction is carried out under kinetic conditions (at a temperature of −45 °C) and the two starting adducts **M1-S** and **M1-R** can interconvert easily, the stereoselective character of the reaction and the *ee* are determined by the energy difference (2.09 kcal mol^{-1}) between the two diastereomeric transition states **TS1-R** and **TS1-S** leading to the two products (*R*)-**1c** and (*S*)-**1c**, respectively.

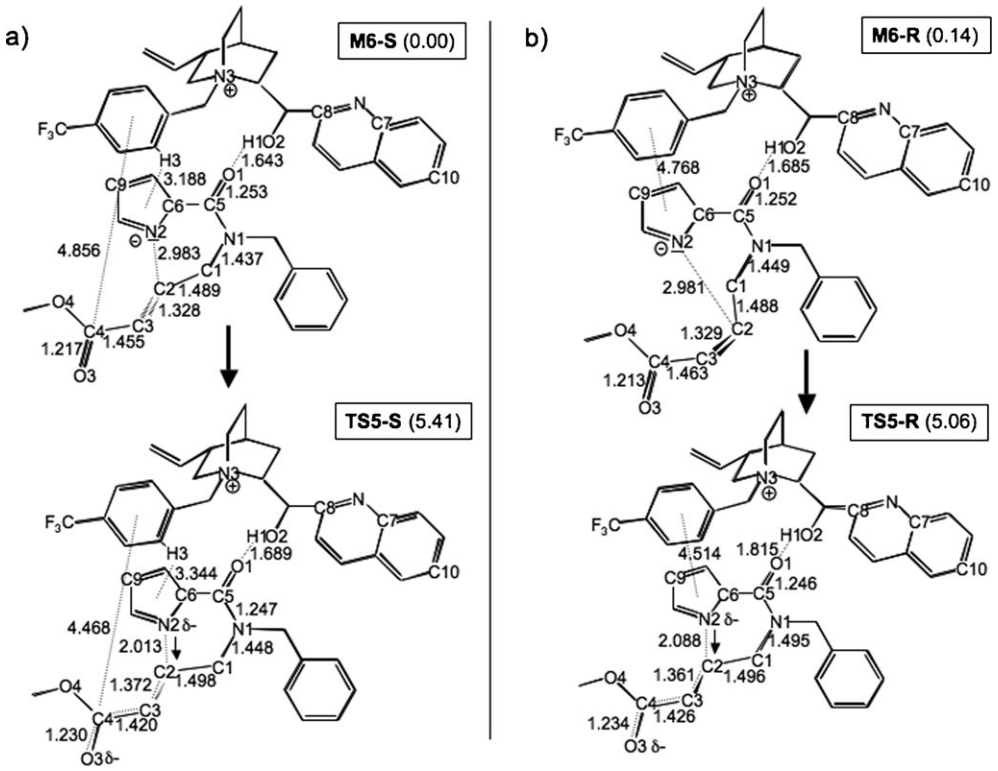

Figure 7. A schematic representation of **M6-S**, **M6-R**, and the two corresponding transition states, **TS4-S** and **TS4-R**. Bond lengths are in Å. When not connecting atoms, dashed lines connect the ring centroids.

The key structural features that are responsible for the **TS1-R/TS1-S** energy difference (favoring **TS1-S**) have been identified. These are: 1) the hydrogen bond O1···H1 between substrate and catalyst; 2) the conformation of the substrate amino-propene unit; and 3) a complex interplay of the π-stacking interactions involving different groups of substrate and catalyst. In particular, we have found that the π interaction between the indole and the benzyl–CF_3 groups is crucial.

The key-role played by this interaction has been demonstrated clearly by the computations carried out on the model systems emulating the pyrrole-analogous **3l** and **3m.** In these cases the lack of interactions between the indole (replaced by the pyrrolyl group) and the benzyl–CF_3 fragment determines a significant decrease in the energy difference between the two diastereomeric pathways.

The mechanistic picture based on the above-mentioned nonbonded interaction has been fully corroborated by control experiments on tailored acyclic precursors. These results also nicely account for the moderate stereochemical levels obtained with pyrrolyl derivatives **3l** and **3m** (*ee* up to 56%) for which the crucial π–π interaction between the larger indolyl core and the CF_3-substitued benzyl group of the catalyst is missing. Efforts toward the exploitation of these findings in the rational design of new chiral PT-catalysts for intramolecular aza-Michael of pyrrolyl derivatives are in progress.

Experimental Section

General methods: ^{1}H NMR spectra were recorded on Varian 200 (200 MHz) and Varian 300 (300 MHz) spectrometers. Chemical shifts are reported in ppm from TMS with the solvent resonance as the internal standard (deuterochloroform: $\delta = 7.27$ ppm). Data are reported as follows: chemical shift, multiplicity (s = singlet, d = duplet, pd = pseudo duplet, t = triplet, q = quartet, br = broad, brs = broad singlet, m = multiplet), coupling constants (Hz). ^{13}C NMR spectra were recorded on Varian 200 (50 MHz) or Varian 300 (75 MHz) spectrometers with complete proton decoupling. Chemical shifts are reported in ppm from TMS with the solvent as the internal standard (deuterochloroform: $\delta = 77.0$ ppm). GC–MS spectra were taken by EI ionization at 70 eV on a Hewlett–Packard 5971 with GC injection. LC-electrospray ionization mass spectra were obtained using an Agilent Technologies MSD1100 single-quadrupole mass spectrometer. Chromatographic purification was performed with 240–400 mesh silica gel. Precoated preparative TLC plates were purchased from FLUKA (silica gel 60 F254). Elemental analyses were carried out by using an EACE 1110 CHNOS analyzer. Analytical high performance liquid chromatography (HPLC) was performed on a liquid chromatograph equipped with a variable wavelength UV detector (deuterium lamp 190–600 nm), using a Daicel Chiracel™ OD or AD column (0.46 cm I.D. × 25 cm) (Daicel Inc. HPLC grade isopropanol and hexane were used as the eluting solvents). Separation through preparative HPLC was performed on an Agilent Technologies MSD 1100 liquid chromatograph using a Zorbax Eclipse SDB-C18 column (21.2 × 150 mm) with acetonitrile and milliQ-H_2O as eluents. Optical rotations were determined in a 1 mL cell with a path length of 10 mm (Na_D line). Melting points were determined with Bibby Stuart Scientific Melting Point Apparatus SMP3 and are not corrected. Compound **3l** was obtained as previously described.[15] Because the catalyst–substrate adducts examined here involve different aromatic groups, it is reasonable to believe that the interactions involving their π systems should play a key role in the reaction. Consequently, it is mandatory to choose an appropriate method for their de-

scription. Unfortunately, this class of interactions cannot be correctly treated by the most popular DFT functionals (for instance, B3LYP), which are inaccurate for interactions where medium-range correlation effects are dominant.[21] Even if π–π interactions can be satisfactorily described by the MP2 method, this approach is unfeasible for the large model system used here, because it would require too much CPU time for practical and extensive usage. However, a new hybrid functional (denoted as MPWB1K) has recently been proposed by Trulhar.[22] This functional has been demonstrated to be capable of treating medium-range correlation effects and to provide a good estimate of the π–π interactions and reaction energetics[23,24] using reasonable amounts of CPU time. Thus, all DFT computations reported in the present paper were carried out with the Gaussian 03 series of programs[25] using the MPWB1K[22] functional and the DZVP basis set.[26] The DZVP basis is a local spin density (LSD)-optimized basis set of double-zeta quality, which includes polarization functions and is suitable for describing weak hydrogen bonds and π interactions such as those occurring in the system investigated here. The transition vector of the various transition states was analyzed by means of frequency computations.

Typical procedure for the PTC intramolecular aza-Michael addition (1i and 1j): A sample vial was charged with reagent grade toluene (6 mL), the indolyl-ester **3** (50 μmol) and catalyst **4a** (3 mg, 5 μmol). An aqueous solution of KOH (25%, 6 μL, 0.5 equiv) was added to this mixture by syringe, and immediately cooled to −45 °C. The reaction was stirred at the same temperature for 16 h, then the solvent was evaporated under reduced pressure. The crude product was purified directly through a pad of silica.

(*S*)-Ethyl-2-[2-(4-methoxybenzyl)-1-oxo-1,2,3,4-tetrahydropyrazino[1,2-*a*]indol-4-yl]acetate (1i): Yellow solid; flash chromatography (*c*-Hex/AcOEt = 8:2); m.p. 78.5–80.8 °C; yield: 97%; *ee* = 90%; $[\alpha]_D = +4.6$ (*c* = 0.9 in chloroform); HPLC analysis: AD column (214 nm), 40 °C, method: *n*-Hex/IPA = 70:30, flow 1.0 mL min^{-1}, $t_{(S)} = 15.9$ min, $t_{(R)} = 23.0$ min; ^{1}H NMR (300 MHz, [D]CHCl$_3$): $\delta = 1.19$ (t, ^3J(H,H) = 7.2 Hz, 3H), 2.50–2.53 (m, 2H), 3.59 (d, ^3J(H,H) = 13.2 Hz, 1H), 3.80, (s, 3H), 3.90–4.02 (m, 3H), 4.12 (d, ^3J(H,H) = 14.2 Hz, 1H), 4.89–4.91 (m, 1H), 5.14 (d, ^3J(H,H) = 14.1 Hz, 1H), 6.87 (d, ^3J(H,H) = 8.7 Hz, 2H) 7.13–7.19 (m, 1H), 7.29–7.32 (m, 5H), 7.71 ppm (d, ^3J(H,H) = 8.1 Hz, 1H); ^{13}C NMR (75 MHz, [D]CHCl$_3$): $\delta = 13.9$, 35.8, 47.2, 48.1, 48.7, 55.2, 61.0, 107.0, 109.5, 114.2, 120.9, 122.9, 124.7, 127.7, 128.3, 128.6, 130.1, 135.3, 159.3, 159.6, 170.4 ppm; ESI-MS: *m*/*z* (%): 393 $[M+1]^+$.

(*S*)-Ethyl-2-[2-(4-fluorobenzyl)-1-oxo-1,2,3,4-tetrahydropyrazino[1,2-*a*]indol-4-yl]acetate (1j): Pale white solid; flash chromatography (*c*-Hex/AcOEt = 8:2); m.p. 88.3–91.7 °C; yield: 85%; *ee* = 84%; $[\alpha]_D = +2.4$ (*c* = 1.7 in chloroform); HPLC analysis: AD column (214 nm), 40 °C, method: *n*-Hex/IPA = 70:30, flow 1.0 mL min^{-1}, $t_{(S)} = 17.3$ min, $t_{(R)} = 28.8$ min; ^{1}H NMR (200 MHz, [D]CHCl$_3$): $\delta = 1.14$ (t, ^3J(H,H) = 7.0 Hz, 3H), 2.52 (d, ^3J(H,H) = 7.4 Hz, 2H), 3.59 (d, ^3J(H,H) = 13.0 Hz, 1H), 3.90–4.07 (m, 3H), 4.87 (d, ^3J(H,H) = 14.6 Hz, 1H), 4.34 (d, ^3J(H,H) = 14.6, 1H), 4.87–4.96 (m, 1H), 5.17 (d, ^3J(H,H) = 14.6 Hz, 1H), 7.01–7.09 (t, ^3J(H,H) = 8.0 Hz, 2H), 7.17 (dt, ^3J(H,H) = 8.0, ^3J(H,H) = 1.8 Hz, 1H), 7.32–7.39 (m, 5H), 7.70 ppm (d, ^3J(H,H) = 8.0 Hz, 1H); ^{13}C NMR (75 MHz, [D]CHCl$_3$) $\delta = 14.2$, 36.0, 47.5, 48.5, 49.0, 61.3, 107.5, 109.8, 116.0 (d, $J = 21.8$ Hz), 121.3, 123.2, 125.1, 128.0, 128.3, 130.8 (d, $J = 7.8$ Hz), 134.2 (d, $J = 206.3$ Hz), 159.9, 162.7 (d, $J = 244.5$ Hz), 170.6 ppm; ESI-MS: *m*/*z* (%): 381 $[M+1]^+$.

Typical procedure for the PTC intramolecular aza-Michael addition (1k): Indolyl ester **3k** (20 mg, 0.07 mmol) was dissolved in toluene (4 mL) in a 10 mL round-bottomed flask equipped with a magnetic stirrer. After the addition of the catalyst **3a** (4 mg, 10 mol%), solid *t*BuOK (8.2 mg, 0.07 mmol) was added. After 1 h stirring at room temperature the starting material was consumed (judged by TLC), and the reaction mixture brought to dryness under vacuum and purified by flash chromatography.

(−)-Ethyl-2-(1-oxo-3,4-dihydro-1H-[1,4]oxazino[4,3-a]indol-4-yl)acetate (1k): Pale yellow viscous oil; flash chromatography (*c*-Hex/AcOEt = 8:2); yield: 75%; *ee* = 59%; $[\alpha]_D = -12.5$ (*c* = 0.4 in chloroform); HPLC analysis: AD column (214 nm), RT, method: *n*-Hex/IPA = 80:20, flow 1.0 mL min^{-1}, $t_{(minor)} = 10.9$ min, $t_{(major)} = 13.3$ min; ^{1}H NMR (300 MHz, [D]CHCl$_3$): $\delta = 1.27$ (t, ^3J(H,H) = 7.2 Hz, 3H), 2.81 (dd, ^3J(H,H) = 4.8 Hz, ^3J(H,H) = 12.0 Hz, 1H), 3.02 (dd, ^3J(H,H) = 16.8 Hz, ^3J(H,H) = 9.3 Hz, 1H), 4.13–4.26 (m, 2H), 4.81 (s, 2H), 5.06 (br, 1H), 7.21–7.31 (m, 2H), 7.46 (s, 2H), 7.51 (s, 1H), 7.80 ppm (d, ^3J(H,H) = 8.1 Hz, 1H); ^{13}C NMR (50 MHz, [D]CHCl$_3$): $\delta = 14.1$, 35.8, 47.3, 61.5, 69.7, 110.1, 111.1, 121.8, 122.8, 123.5, 126.5, 127.2, 135.8, 159.3, 170.3 ppm; ESI-MS: *m*/*z* (%): 274 $[M+1]^+$.

Typical procedure for the PTC intramolecular aza-Michael addition (1l and 1m): Method A: A sample vial was charged with reagent grade toluene (6 mL), the indolyl-ester **3l or 3m** (50 μmol) and catalyst **4a** (3 mg, 5 μmol). An aqueous solution of KOH (25%, 6 μL, 0.5 equiv) was added to the mixture by syringe and immediately cooled to −45 °C. The reaction was stirred at the same temperature for 16 h, then the solvent was evaporated under reduced pressure. The crude product was purified directly through a pad of silica. Method B: same conditions but at RT.

Data for 1l:[15] Yield: 82%; flash chromatography (*c*-Hex/AcOEt = 8:2); *ee* = 54%; $[\alpha]_D = -20.1$ (*c* = 1.3 in chloroform); HPLC analysis: OD column (210 nm), RT, method: *n*-Hex/IPA = 90:10, flow 1.0 mL min^{-1}, $t_{(major)} = 21.3$ min, $t_{(minor)} = 25.6$ min.

Data for 1m:[15] Yield: 77%; flash chromatography (*c*-Hex/AcOEt = 85:15); *ee* = 56%; $[\alpha]_D = +4.6$ (*c* = 1.5 in chloroform); HPLC analysis: OD column (214 nm), RT, method: *n*-Hex/IPA = 90:10, flow 1.0 mL min^{-1}, $t_{(minor)} = 14.9$ min, $t_{(major)} = 19.4$ min.

Acknowledgements

Acknowledgement is made to the MIUR (Rome), FIRB Project (Progettazione, preparazione e valutazione biologica e farmacologica di nuove molecole organiche quali potenziali farmaci innovativi), Università di Bologna and Fondazione del Monte di Bologna e Ravenna.

[1] a) D. J. Faulkner, *Nat. Prod. Rep.* **2002**, *19*, 1–48; b) A. Kleeman, J. Engel, B. Kutscher, D. Reichert, *Pharmaceutical Substances*, 4th ed., Thieme, New York, **2001**; c) J. Sundberg, *Pyrroles and Their Benzoderivatives: Synthesis and Applications in Comprehensive Heterocyclic Chemistry, Vol. 4* (Eds.: A. R. Katritzky, C. W. Rees), Pergamon, Oxford, **1984**, pp. 313–376; d) A. Joule, *Indole and its Derivatives in Science of Synthesis: Houben-Weyl Methods of Molecular Transformations, Vol. 10* (Ed.: E. J. Thomas), Thieme, Stuttgart, **2000**; Chapter 10.13.

[2] a) G. W. Gribble, *J. Chem. Soc. Perkin Trans. 1* **2000**, 1045–1075; b) R. Dalpozzo, G. Bartoli, *Curr. Org. Synth.* **2005**, *2*, 163–178; c) S. Cacchi, G. Fabrizi, *Chem. Rev.* **2005**, *105*, 2873–2920; d) G. W. Gribble, M. G. Saumier, E. T. Pelkey, T. L. S. Kishbaugh, Y. Liu, J. Jiang, H. A. Trujillo, D. J. Keavy, D. A. Davis, S. C. Conway, F. L. Switzer, S. Roy, R. A. Silva, J. A. Obaza-Nutatis, M. P. Sibi, N. V. Moskalev, T. C. Barden, L. Chang, W. M. Habeski, B. Pelcman, W. R. Sponholtz III, R. W. Chau, B. D. Allison, S. D. Garaas, M. S. Sinha, M. A. McGowan, M. R. Reese, K. S. Harpp, *Curr. Org. Chem.* **2005**, *9*, 1493–1519; e) S. Agarwal, S. Cämmerer, S. Filali, W. Froöhner, J. Knöll, M. P. Krahl, K. R. Reddy, H.-J. Knölker, *Curr. Org. Chem.* **2005**, *9*, 1601–1614; f) M. Bandini, A. Melloni, S. Tommasi, A. Umani-Ronchi, *Synlett* **2005**, 1199–1222; g) G. R. Humphrey, J. T. Kuethe, *Chem. Rev.* **2006**, *106*, 2875–2911; h) J. Campo, M. Garcìa-Valverde, S. Marcaccini, M. J. Rojo, T. Torroba, *Org. Biomol. Chem.* **2006**, *4*, 757–765.

[3] a) K. A. Jørgensen, *Synthesis* **2003**, 1117–1125; b) M. Bandini, A. Melloni, A. Umani-Ronchi, *Angew. Chem.* **2004**, *116*, 560–566; *Angew. Chem. Int. Ed.* **2004**, *43*, 550–556; c) M. Bandini, E. Emer, S. Tommasi, A. Umani-Ronchi, *Eur. J. Org. Chem.* **2006**, 3527–3544; d) Y.-F. Sheng, A.-J. Zhang, X.-J. Zheng, S.-L. You, *Chin. Org. Chem.* **2008**, *28*, 605–616; e) B. Poulsen, K. A. Jørgensen, *Chem. Rev.* **2008**, *108*, 2903–2915; f) S.-L. You, C. Quan, Z. Mi, *Chem. Soc. Rev.* **2009**, *38*, 2190–2201; g) M. Rueping, B. J. Nachtsheim, *Beilstein J. Org. Chem.* **2010**, *6*, DOI: 10.3762/bjoc.6.6.

[4] *Catalytic Asymmetric Friedel–Crafts Alkylations* (Eds.: M. Bandini, A. Umani-Ronchi), Wiley-VCH, Weinheim, **2009**.

[5] a) D. A. Evans, K. R. Fandrick, *Org. Lett.* **2006**, *8*, 2249–2252; b) D. A. Evans, K. R. Fandrick, H.-J. Song, K. A. Scheidt, R. Xu, *J. Am. Chem. Soc.* **2007**, *129*, 10029–10041; c) G. Blay, I. Fernández, J. R. Pedro, C. Vila, *Tetrahedron Lett.* **2007**, *48*, 6731–6734; d) G. Blay, I. Fernández, J. R. Pedro, C. Vila, *Org. Lett.* **2007**, *9*, 2601–2604; e) Q. Kang, X.-J. Zheng, S.-L. You, *Chem. Eur. J.* **2008**, *14*, 3539–3542; f) M. Zeng, Q. Kang, Q. Kang, Q.-L. He, S.-L. You, *Adv. Synth. Catal.* **2008**, *350*, 2169–2173; g) Y.-F. Sheng, G.-Q. Li, Q. Kang, A.-J. Zhang, S.-L. You, *Chem. Eur. J.* **2009**, *15*, 3351–3354.

[6] a) J. J. Vepsäläinen, S. Auriola, M. Tukiainen, N. Ropponen, Callaway, *J. Planta Med.* **2005**, *71*, 1049–1057; b) A. L. Williams, J. M. Srinivasan, J. N. Johnston, *Org. Lett.* **2006**, *8*, 6047–6049; c) S. Grüschow, L. C. Chang, Y. Mao, D. H. Sherman, *J. Am. Chem. Soc.* **2007**, *129*, 6470–6476, and references therein; d) M. B. Johansen, M. A. Kerr, *Org. Lett.* **2008**, *10*, 3497–3500; e) S. Chamberland, S. Grueschow, D. H. Sherman, R. M. Williams, *Org. Lett.* **2009**, *11*, 791–794.

[7] a) D. Moffat, C. J. Nichols, D. A. Riley, N. S. Simpkins, *Org. Biomol. Chem.* **2005**, *3*, 2953–2975; b) E. Wincent, H. Shirani, J. Bergman, U. Rannug, T. Janosik, *Bioorg. Med. Chem.* **2009**, *17*, 1648–1653.

[8] a) B. M. Trost, M. J. Krische, V. Berl, E. M. Grenzer, *Org. Lett.* **2002**, *4*, 2005–2008; b) For an analogous approach on pyrrole derivatives, see: B. M. Trost, G. Dong, *Chem. Eur. J.* **2009**, *15*, 6910–6919; c) L. M. Stanley, J. F. Hartwig, *Angew. Chem.* **2009**, *121*, 7981–7984; *Angew. Chem. Int. Ed.* **2009**, *48*, 7841–7844.

[9] a) H.-L. Cui, X. Feng, J. Peng, J. Lei, K. Jiang, Y.-C. Chen, *Angew. Chem.* **2009**, *121*, 5847–5850; *Angew. Chem. Int. Ed.* **2009**, *48*, 5737–5740; b) D. Enders, C. Wang, G. Raabe, *Synthesis* **2009**, 4119–4124.

[10] a) M. Bandini, A. Eichholzer, *Angew. Chem.* **2009**, *121*, 9786–9824; *Angew. Chem. Int. Ed.* **2009**, *48*, 9608–9644, and references therein; b) M. Bandini, A. Eichholzer, *Angew. Chem.* **2009**, *121*, 9697–9701; *Angew. Chem. Int. Ed.* **2009**, *48*, 9533–9537.

[11] M. Bandini, A. Eichholzer, M. Tragni, A. Umani-Ronchi, *Angew. Chem.* **2008**, *120*, 3282–3285; *Angew. Chem. Int. Ed.* **2008**, *47*, 3238–3241.

[12] a) F. Cafieri, E. Fattorusso, O. Tagliatela-Scafati, *J. Nat. Prod.* **1998**, *61*, 122–125, and references therein; b) K. G. Poullennec, D. Romo, *J. Am. Chem. Soc.* **2003**, *125*, 6344–6345; c) N. Nettekoven, J.-M. Plancher, H. Richter, O. Roche, S. Taylor, PCT Int. Appl. WO US 2007/0135416A1, **2007**.

[13] a) J. M. Bentley, P. Hebeisen, M. Muller, H. Richter, S. Roever, P. Mattei, S. Taylor, PCT Int. Appl. WO 2001-EP8520 20010724, **2002**; b) R. K. Tiwari, A. K. Verma, A. K. Chhillar, D. Singh, J. Singh, V. K. Sankar, V. Yadav, G. L. Sharma, R. Chandra, *Bioorg. Med. Chem.* **2006**, *14*, 2747–2752.

[14] a) J. Patel, N. Pelloux-LIon, F. Minassian, Y. VallIe, *J. Org. Chem.* **2005**, *70*, 9081–9084; b) J. Patel, N. Pelloux-LIon, F. Minassian, Y. VallIe, *Tetrahedron Lett.* **2006**, *47*, 5561–5563.

[15] M. Bandini, A. Eichholzer, M. Monari, F. Piccinelli, A. Umani-Ronchi, *Eur. J. Org. Chem.* **2007**, 2917–2920.

[16] For general reviews see: a) A. Nelson, *Angew. Chem.* **1999**, *111*, 1685–1687; *Angew. Chem. Int. Ed.* **1999**, *38*, 1583–1585; b) B. Lygo, B. I. Andrews, *Acc. Chem. Res.* **2004**, *37*, 518–525; c) L.-W. Xu, C.-G. Xia, *Eur. J. Org. Chem.* **2005**, 633–639, and references therein; d) A. Berkessel, H. Gröger in *Asymmetric Organocatalysis*, Wiley-VCH, Weinheim, **2005**; e) T. Ooi, K. Maruoka, *Aldrichimica Acta* **2007**, *40*, 77–86; f) J. L. Vicario, D. Badia, L. Carrillo, *Synthesis* **2007**, 2065–2092, and references therein; g) H. Pellissier, *Tetrahedron* **2007**, *63*, 9267–9331; h) K. Maruoka, *Asymmetric Phase Transfer Catalysis*, Wiley-VCH, Weinheim, **2008**; i) K. Maruoka, *Org. Process Res. Dev.* **2008**, *12*, 679–697; <**lit** l>K. Maruoka, *Synlett* **2009**, 652–652.

[17] For representative examples see: a) K. Tajasu, S. Maiti, M. Ihara, *Heterocycles* **2003**, *59*, 51–55; b) S. Fustero, D. Jiménez, J. Moscardó, S. Catalán, C. del Pozo, *Org. Lett.* **2007**, *9*, 5283–5286; c) S. K. Bur, A. Pawda, *Adv. Heterocycl. Chem.* **2007**, *94*, 1–105; d) E. C. Carlson, L. K. Rathbone, H. Yang, N. D. Collet, R. G. Carter, *J. Org. Chem.* **2008**, *73*, 5155–5158; e) S. Fustero, J. Moscardó, D. Jiménez, M. D. Pérez-Carrion, M. Sanchez-Roselló, C. del Pozo, *Chem. Eur. J.* **2008**, *14*, 9868–9872; f) *Asymmetric Synthesis of Nitrogen Heterocycles*, (Ed.: J. Royer), Wiley-VCH, Weinheim, **2009**, and references therein.

[18] For representative examples: a) U.-H. Dolling, P. Davis, E. J. J. Grabowski, *J. Am. Chem. Soc.* **1984**, *106*, 446–447; b) D. L. Hughes, U.-H. Dolling, K. M. Ryan, E. F. Schoenewaldt, E. J. J. Grabowski, *J. Org. Chem.* **1987**, *52*, 4745–4752; c) E. J. Corey, F. Xu, M. C. Noe, *J. Am. Chem. Soc.* **1997**, *119*, 12414–12415; d) E. J. Corey, Y. Bo, J. Busch-Petersen, *J. Am. Chem. Soc.* **1998**, *120*, 13000–13001; e) T. Ooi, M. Kameda, M. Taniguchi, K. Maruoka, *J. Am. Chem. Soc.* **2004**, *126*, 9685–9694; f) A. Berkessel, M. Guixà, F. Schmidt, J. M. Neudörfl, J. Lex, *Chem. Eur. J.* **2007**, *13*, 4483–4498.

[19] F. Bernardi, A. Bottoni, G. Tonachini, *J. Chem. Soc. Perkin Trans. 2* **1980**, 467–470.

[20] Obtained with an analogous **4a** ammonium salt in which the CF_3 group at the benzylic pendant was replaced by a NO_2 group.

[21] Y. Zhao, D. G. Truhlar, *Acc. Chem. Res.* **2008**, *41*, 157–167.

[22] Y. Zhao, D. G. Truhlar, *J. Phys. Chem. A* **2004**, *108*, 6908–6918.

[23] Y. Zhao, D. G. Truhlar, *J. Phys. Chem. A* **2005**, *109*, 5656–5667.

[24] Y. Zhao, O. Tishchenko, D. G. Truhlar, *J. Phys. Chem. B* **2005**, *109*, 19046–19051.

[25] Gaussian 03, Revision C.02, M. J. Frisch, G. W. Trucks, H. B. Schlegel, G. E. Scuseria, M. A. Robb, J. R. Cheeseman, J. A. Montgomery, Jr., T. Vreven, K. N. Kudin, J. C. Burant, J. M. Millam, S. S. Iyengar, J. Tomasi, V. Barone, B. Mennucci, M. Cossi, G. Scalmani, N. Rega, G. A. Petersson, H. Nakatsuji, M. Hada, M. Ehara, K. Toyota, R. Fukuda, J. Hasegawa, M. Ishida, T. Nakajima, Y. Honda, O. Kitao, H. Nakai, M. Klene, X. Li, J. E. Knox, H. P. Hratchian, J. B. Cross, V. Bakken, C. Adamo, J. Jaramillo, R. Gomperts, R. E. Stratmann, O. Yazyev, A. J. Austin, R. Cammi, C. Pomelli, J. W. Ochterski, P. Y. Ayala, K. Morokuma, G. A. Voth, P. Salvador, J. J. Dannenberg, V. G. Zakrzewski, S. Dapprich, A. D. Daniels, M. C. Strain, O. Farkas, D. K. Malick, A. D. Rabuck, K. Raghavachari, J. B. Foresman, J. V. Ortiz, Q. Cui, A. G. Baboul, S. Clifford, J. Cioslowski, B. B. Stefanov, G. Liu, A. Liashenko, P. Piskorz, I. Komaromi, R. L. Martin, D. J. Fox, T. Keith, M. A. Al-Laham, C. Y. Peng, A. Nanayakkara, M. Challacombe, P. M. W. Gill, B. Johnson, W. Chen, M. W. Wong, C. Gonzalez, J. A. Pople, Gaussian, Inc., Wallingford CT, **2004**.

[26] N. Godbout, D. R. Salahub, J. Andzelm, E. Wimmer, *Can. J. Chem.* **1992**, *70*, 560–571.

Received: March 3, 2010
Published online: September 13, 2010

